Machine-Learning Discovery of Highly Oxidized IrO_x Phases

Raul A. Flores,[*,†] Christopher Paolucci,[*,‡] Ankit Jain,[*,¶] Muratahan Aykol,[*,§] Jens K. Nørskov,[*,¶] Michal Bajdich,[*,‖] and Thomas Bligaard[*,‖]

† *SUNCAT Center for Interface Science and Catalysis, Department of Chemical Engineering, Stanford University, Stanford 94305, California, USA*

‡ *Department of Chemical Engineering, University of Virginia, Charlottesville, Virginia 22903, United States*

¶ *Department of Physics, Technical University of Denmark, Lyngby, Denmark*

§ *Toyota Research Institute, Los Altos, CA 94022, USA*

‖ *SUNCAT Center for Interface Science and Catalysis, SLAC National Accelerator Laboratory, Menlo Park, CA 94025, USA*

E-mail: flores12@stanford.edu; cp9wx@virginia.edu; temp_temp_ankits_email_address_temp_temp@dtu.dk; muratahan.aykol@tri.global; jkno@dtu.dk; bajdich@slac.stanford.edu; bligaard@stanford.edu

Abstract

Recent advancements in statistical methods, colloquially termed as machine learning, have revolutionized a tremendous number of fields due to the ease by which we can train models that are flexible enough to regress to data of interest while maintaining predictive power. Nowhere has this this impact been felt as much as in the field of materials science, which had previously been bottle-necked by relatively computationally expensive methods. Herein, we report on a ML methodology to enumerate bulk

crystal structures in the IrO_2 and IrO_3 space.

Introduction

Iterative Active Machine Learning and unique prototype identification to discover stable new materials and catalysts. Motivation for IrO_x, low representation, longstanding controversy over oxidation states and topology, and demonstrates promise for OER and Li ion batteries.

Reported +6 oxidation state phases are achievable leading to high degree of structural variability, which is the highest for transition metals. High oxidation states (low pH high anodic voltage, harsh oxidizing conditions) unexplored, need very specific structures with precise oxygen connectivity (aka high pressure $SrIrO_3$) that can exist. Machine learning is the efficient way to explore this exploring Antarctica for life sparse space. What we show here...

The two key features of our algorithm that make the exporation of an expanseive space possible are its use of surrogate models and active learning framework. Because DFT calculations are prohibitebly computationally expensive to carry out for large data sets, herein we train a Gaussian Process (GP) machine learning model to serve as a surrogate model. In general active learning applciations, the requisite training data is not available. Active learning frameworks are a means by which to generate the most valuable training data set, on the fly.

Oxides for batteries/fuel cells, Iridium Oxide, OER, Lithiated IrO_3. Highly oxidized phases of oxides for fuel cell and energy storage applications.

Results and discussion

I. IrO_2

The structures that comprise the candidate data set were constructed by parsing for structurally unique systems in the OQMD and Materials Project DFT databases. The structural uniqness was performed using a space-group symmetry classification scheme developed by TEMP-Ankit-REF which can classify any arbitrary structure based on stoicheomtetry (composition), space-group, and Wycoff positionining of the atoms (see SI for more details on the structural classification scheme). To focus the scope of the study, only AB2 and AB3 stoicheometries were parsed from the databased. The AB2 formula was chosen because it includes rutile-IrO_2 , the known most stable polymorph of IrO2. Importantly, AB3 was chosen to include high valency IrO3 structures in our search. This classification scheme can directly serve as a fingerprinting scheme and has succesffuly been used for the prediction of formation energies. The results of the classification scheme resulted in a XYZ AB2 and XYZ AB3 structural prototypes for which iridium and oxygen were replaced for A and B sites, respectively. Finally, a coarse isotropic volume relaxation based on atomic radii was performed on the structures to accomodate the atomic radii of iridium and oxygen into the lattice. Finally, a Vornoi tesselation based fingerprinting scheme developed by Wolverton-paper-REF was used to encode the relevent chemcial information for each structure. The Voronoi based method was used because it is insensitive to volume relaxation. PCA was used to reduce the dimensionality of the feature space from 271 to 20 features such that 99percent of the variance is captured.

The active learning algorithm proceeds through iterative ML training, prediction, and aqusition steps and is visualized in figure TEMP. The A Gaussian process (GP) regression employing a rational quadratic kernal was chosen as the ML model because it offers a high degree of flexibility and importantly, error quantification for the predicted formation energies. Further details on the GP model, including hyper parameter information, is including in the

SI.

1. Candidate space of structures is generated
2. Initial seed data is used to train a ML model
3. ML model predicts energy of entire candidate space
4. Most valuable calculation(s) is selected using aquisition function
5. DFT calculation(s) is(are) performed to obtain additional training data points
6. ML model is retrained with additional data
7. Repaet steps (TEMP) through (TEMP) until convergence criteria is reached

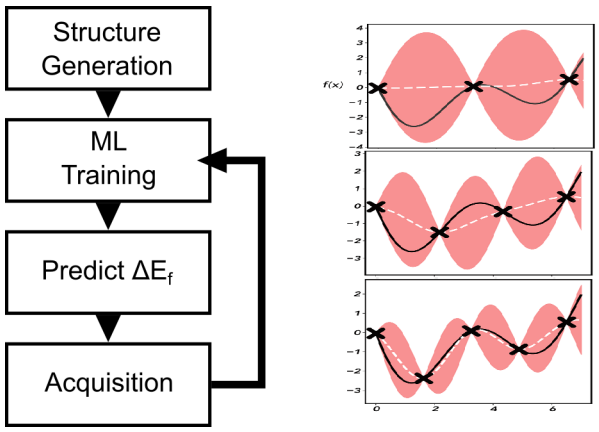

Figure 1: (a) Active learning algorithm diagram. First the candidate space of structures is generated, next, the machine learning model is trained on any available DFT formation energy data. The trained ML model is then used to predict the DE of the entire candidate space. Finally, an aquisition step is performed to pick the next most valuable calcation to perform an-initio DFT on (b) Toy model demonstrating a GP model converging with each subsequent iteration.

II. IrO_3

- Describe relevant features - Physical intuition? - Describe convex hull plot (energy vs. Ir-O distance), computed amorphous phase to define synthesizability - While only 2 IrO_2 in MP/OQMD, we can compare our structures to other computed IrO_2 not in open databases.

This is a citation example.[1]

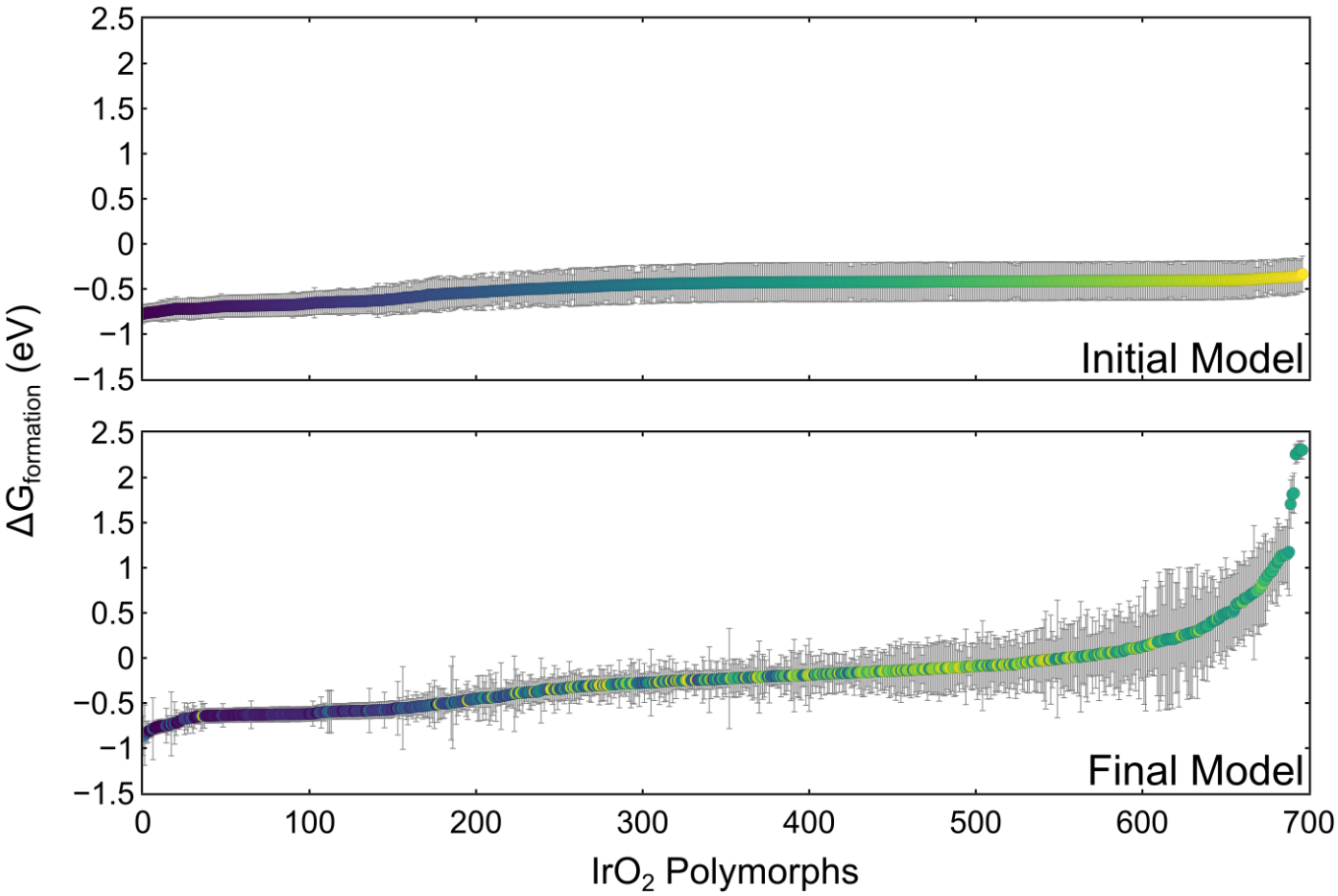

Figure 2: Gaussian process machine learning models trained initially on (a) publically available DFT data for IrO2 and (b) all of the aquired DFT calculations from the active learning algorithm. See SI for additional panels at intermediate iterations of the active learning algorithm. The Gibbs formation energy (either DFT derived or predicted from the GP model) and associated GP estimated error (2 sigmas or something TEMP) is plotted for each polymorph in the IrO2 candidate space. The data points in each subset are ordered from most to least stable (lowest to largest DE formation). The individual markers are colored based on their ordering in the final converged GP model. Aquired structures are identified by their red borders and slightly larger size. The insets show the most stable TEMP structures, where several well known crystal structures are labeled.

- XYZ unique AB3 Structures, 259 unique prototypes. Substitute Ir and O, expand to minimum Ir-O distance ¿ XYZ - followed same procedure as in 3.1, Training Set of 35 structures, 8 of which are IrO_3 - Describe initial training and training after first 10 DFT structures

- Describe convex hull, classes of structures ($\alpha-AlF_3$ like, rutile like, and layered, should

be segregated in hull plot) - briefly describe structures within each class, cite in literature where appropriate

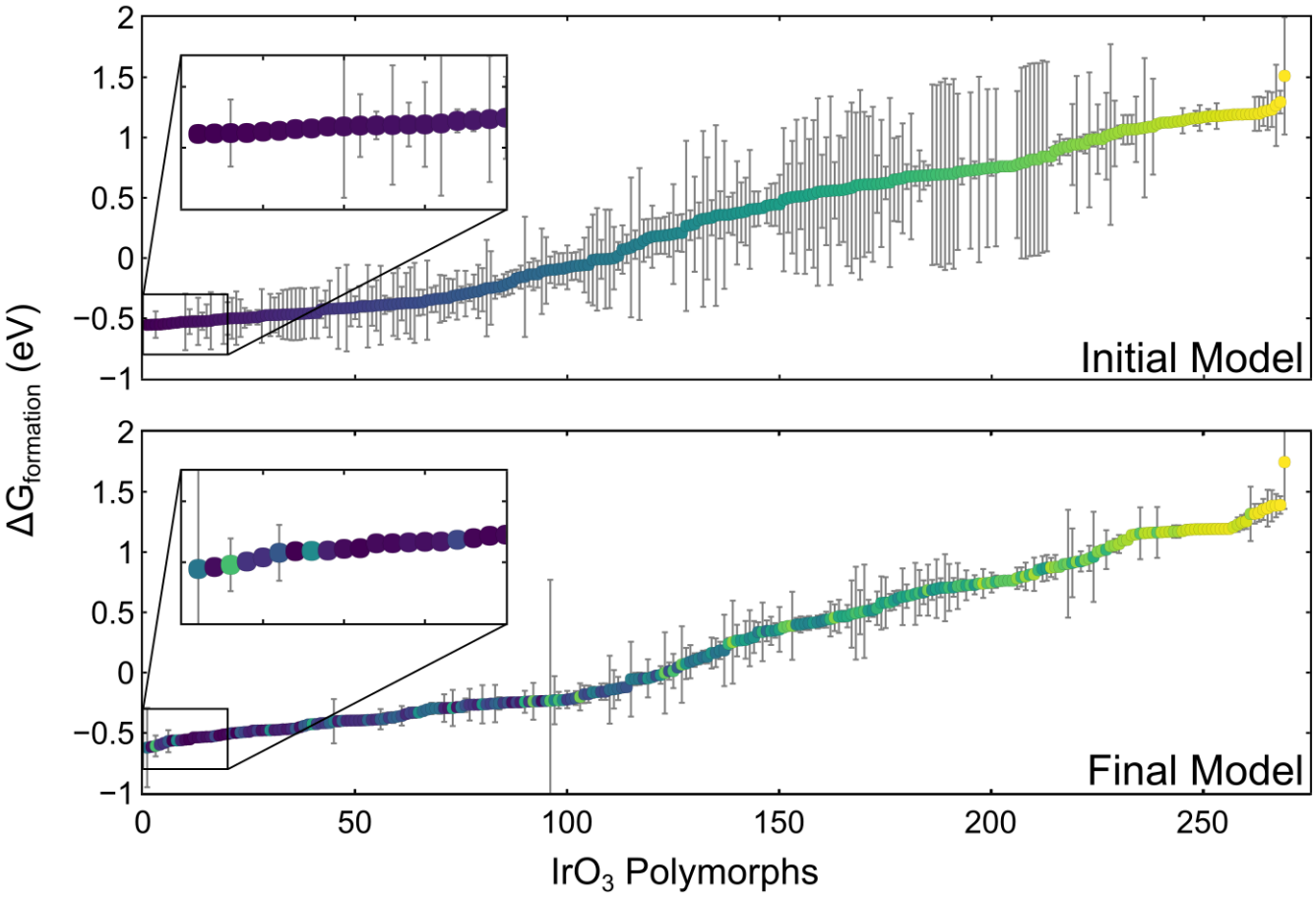

Figure 3: TEMP.

III. Electrochemical OER Application

In the following section we will demonstrate the merit of our stable polymorph discovery algorithm by elucidating the electrochemical properties of the four promising structures discussed in the previous section. In particular, surfaces constructed from the four polymorphs will be evaluated for their activity towards the oxygen evolution reaction (OER), an important chemistry with direct application to fuel cell devices. Additionally, the surfaces will be evaluated for their stability and equilibrium surface coverage of surface oxygen and hydroxides.

Bulk Pourbaix

The electrochemical stability phase diagram (E vs. pH) was constructed by considering the equilibrium conditions of the following species: Ir, rutile-IrO_2 , α-IrO_3 , rutile-IrO_3, β-IrO_3, and an aqueous dissolved IrO[4−] species (See TEMP—SI for additional details). The resulting diagram is shown in Fig. 4. Importantly, under acidic conditions (pH ¡ 7) and in the bias region of interest for the OER (1.23 V vs. RHE) α-IrO_3 shows a large window of stability. This indicates that the α-IrO_3 phase may be stabilized under the highly oxidizing conditions of the OER. The stability regions for rutile-$IrO_3$and β-IrO_3in the absence of any other IrO_3 polymorphs are also indicated by the unfilled solid lines and demonstrate a sizable stability window as well. This result implies that these metastable phases may also play a role for the OER.

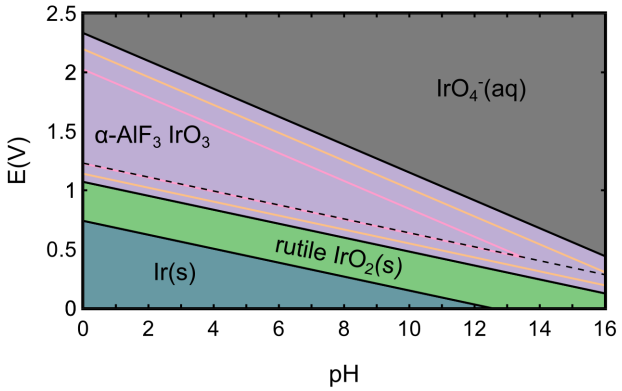

Figure 4: Electrochemical bulk phase stability diagram (Pourbaix) of the Ir-O-H chemical space considering rutile-IrO_2,

b. OER Activities and Surfaces

The OER activity (expressed in terms of the limiting potential) for various surfaces cut from rutile-IrO_2, and the three polymorphs of IrO_3 considered are shown in Fig. 5. The specific facets were chosen from the highest intensity x-ray diffraction peaks from powder-diffraction spectra simulated in VESTA, as well as using physical intuition as to which facets would be most physical.

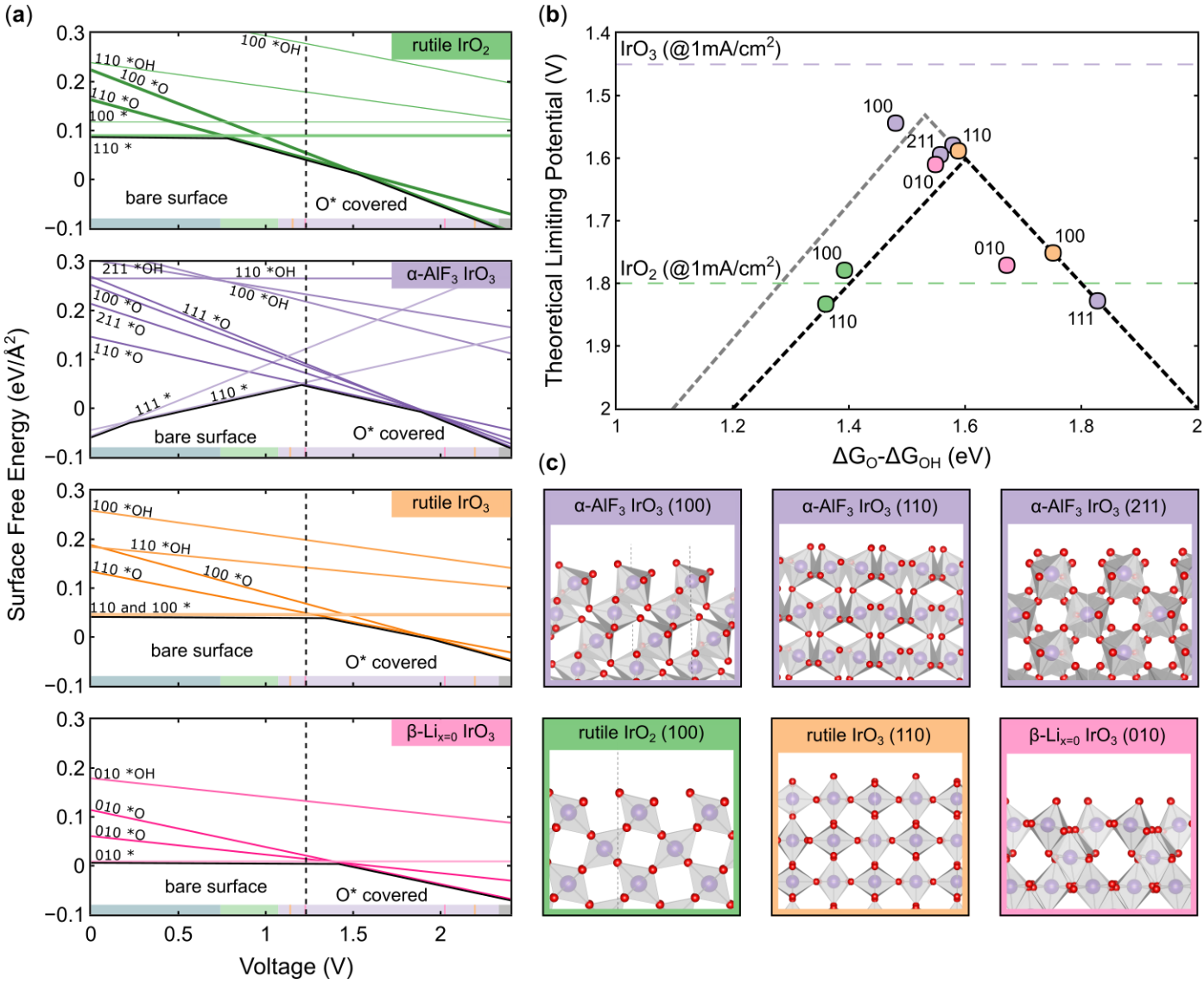

Figure 5: Summary of OER results for the four bulk structures of IrO_x considered: rutile-IrO_2 (green), α-IrO_3 (purple), rutile-IrO_3 (orange), and β-IrO_3 (pink). (a) Surface energy Pourbaix diagrams for each structure, with the surface energy of various facets and coverages shown as a function of applied potential. The bulk Pourbaix diagram's bounds of stability at pH 0 are superimposed at the bottom of each subplot. (b) OER activity volcano for IrO_x systems considered utilizing the ΔG_O -ΔG_{OH} thermodynamic descriptor. The purple dotted line corresponds to the experimental limiting potential at 10 mA cm^2 for IrO_3, while the green band corresponds to the range of experimentally observed overpotentials for pristine IrO_2 catalysts. (c) Select surface facets for the four IrO_x crystal systems considered.

To determine the most likely experimentally abundant surface facets and surface coverages, a surface energy Pourbaix diagram was constructed (TEMP). See (SI for surface energy/Pourbaix part) for the method used to calculate surface energies.

c. OER Intermediate Scaling

Figure TEMP shows the scaling relations between the adsorption free energies of the OER intermediate species for the IrO_x systems studied herein. It can be seen clearly that the data points corresponding to the three IrO_3 polymorphs are roughly 1 eV weaker binding than the rutile-IrO_2 points. This generally weaker binding of the IrO_3 stoichiometry is responsible for the observed improvement in theoretical activity. The ΔG_{OOH} vs.ΔG_{OH} relationship is very close to the traditional "universal scaling relations", demonstrating that our materials do not break the infamous ΔG_{OOH} vs. ΔG_{OH} scaling.

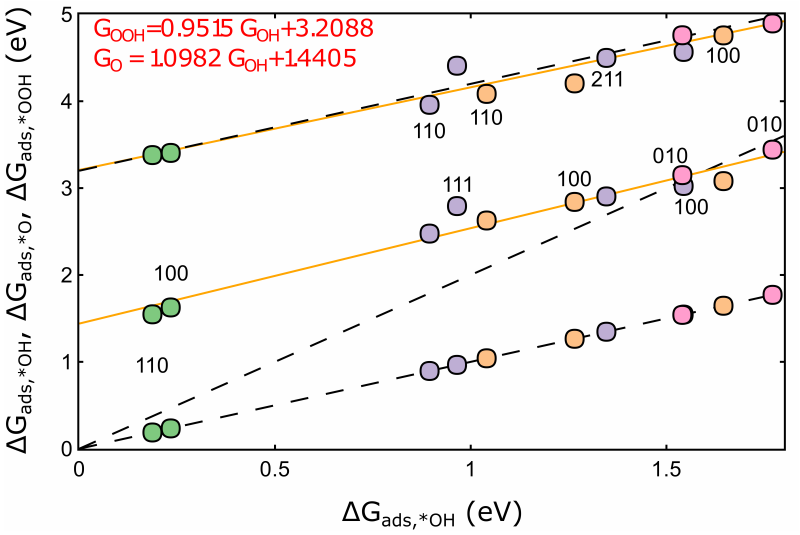

Figure 6: Relationship between the adsorption free energies of the three key OER intermediates (*OH, *O, *OOH), with ΔG_{OH} chosen as the dependent variable. Best fit lines are provided for ΔG_{OOH} vs. ΔG_{OH} and ΔG_O vs. ΔG_{OH} . Additionally, "universal scaling relations" for ΔG_{OOH} vs. ΔG_{OH} and ΔG_O vs. ΔG_{OH} are shown (black dotted lines) to emphasize our deviation from the traditionally reported scaling fits. The trivial ΔG_{OH} vs. ΔG_{OH} relationship is included for completeness.

Conclusion

And in conclusion we presented work here...

Acknowledgement

Organizations to acknowledge TRI SUNCAT Stanford NERSC etc.

JAGT and MB acknowledge the support by the U.S. Department of Energy, Office of Science, Office of Basic Energy Science, via Grant DE-SC0008685 to the SUNCAT Center of Interface Science and Catalysis.

The authors would like to acknowledge the use of the computer time allocation for the Transition metal-oxide and metal surfaces: applications and reactivity trends in catalysis at the National Energy Research Scientific Computing Center, a DOE Office of Science User Facility supported by the Office of Science of the U.S. Department of Energy under Contract No. DE-AC02-05CH11231.

Supporting Information Available

Machine Learning Algorithm Methods

Relevant details about the ML Gaussian process here

Electrochemical OER Computational Methods

Density Functional Theory Methods

All OER calculations were performed using density functional theory (DFT) implemented via the Vienna ab-initio simulation package (VASP) and utilizing the PBE exchange-correlation functional. Dipole corrections were imposed on all non-symmetric slabs. A 4x4x3 k-point mesh with gamma-point centered Monkshort-packing was used for all slabs. The plane-wave energy cutoff was 500 eV.

All slab calculations maintained a vacuum spacing of ¡15 A. All structures were relaxed utilizing a TEMP algorithm with a stop criteria being that all atoms satisfy a maximum force threshold of 0.02 eV/A.

OER Thermodynamic Methodology

Surface Energy Pourbaix Methodology

Procedure: - For the top/most stable bulk structures the following procedure was carried out

* Stable stoicheometric terminations were cut from the bulk Stable termination planes were guesstimated via intuition, and the x-ray diffraction pattern tool from Vesta

* Electrochemical surface coverage was elucidated via a surface Pourbaix analysis Need to know the coverage of surface under operating conditions (¿1.23 V RHE)

* Thermodynamic/limiting potential analysis of the OER mechanistic pathway Volcano plot, limiting potentials, etc.

References

(1) Smith, A.; Smith, J. TEMP title. **9999**, *1*.

Graphical TOC Entry